Ocean Modelling 136 (2019) 13–27

Contents lists available at ScienceDirect

Ocean Modelling

journal homepage: www.elsevier.com/locate/ocemod

Modeling nonlinear tidal evolution in an energetic estuary

Salme E. Cook*, Thomas C. Lippmann, James D. Irish

University of New Hampshire, 24 Colovos Rd., Durham, NH 03824, United States of America

ARTICLE INFO

Keywords:
Numerical modeling
Tidal dissipation
Nonlinear tidal evolution
Gulf of Maine
Hydrodynamic model validation

ABSTRACT

Three-dimensional numerical simulations of a tidally dominated estuary within the Gulf of Maine are performed using the Regional Ocean Modeling System (ROMS) and validated with observations of sea surface elevation and velocity time series obtained between 1975 and 2016. The model is forced at the ocean boundary with tidal constituents (M2, S2, N2, O1, K1), a time series of observed subtidal elevations and discharge from seven rivers that drain into the estuary. Harmonic analysis is used to determine the tidal dissipation characteristics and generation of overtides within the system. Amplitude decay and phase shift of the dominant semidiurnal (M2) tidal component shows good agreement with observations throughout the main channel of the Piscataqua River and over the channels and mudflats of the Great Bay. The model simulates harmonic growth of the overtides across the spectrum, and indicates a spatial evolution of the tide consistent with a shoaling wave that evolves from a skewed elevation profile with ebb dominance in the lower parts of the estuary, to a more asymmetric, pitched-forward shape consistent with flood dominance. The M4 constituent has spatial variation qualitatively similar to the observations but has magnitudes that are under-predicted in the complex bathymetric region of the Piscataqua River where much of the M2 tidal dissipation occurs. The M6 tidal constituent agrees well with the observations throughout the estuary suggesting that frictional effects on harmonic growth are well modeled. Root-mean-square model-data differences in velocities ($\sim 0.05\, m/s$) and sea surface elevation ($\sim 0.1\, m$) agree to within about 10% of the tidal amplitudes. Differences between model simulations with and without subtidal oscillations in the estuary are small, suggesting that interactions between the tide and other low frequency (subtidal) mean flows are weak and can be ignored when considering tidal dynamics. Including average fresh water discharge in the model does not affect the behavior of the tidal flows, but can generate high frequency baroclinic velocities potentially important to mixing within the estuary.

1. Introduction

The transport and mixing of water, sediment, nutrients and organisms in estuarine and coastal systems is often dominated by astronomical tidal forcing. Of particular interest are the dynamics of shoaling tides induced by nonlinear wave interactions and energy dissipation, and how that process impacts long term coastal planning and environmental conservation efforts. As the tide propagates from the open ocean onto the shelf and into estuaries, it becomes progressively more nonlinear and distorted, leading to growth (shoaling) or decay (dissipation) of tidal amplitudes, shifts in the phase of the tide, and growth of tidal harmonics. Resulting tidal currents are difficult to predict analytically over realistic and complex bathymetry, and require observation or numerical simulation to quantify. Evolution of tidal nonlinearities produces asymmetries in ebb/flood current strength and duration (Boon and Byrne, 1981), that when averaged over a tidal cycle has been used to estimate net sediment transport and circulation patterns (Dronkers, 1986); stronger flood currents drive the movement of coarse sediment and longer slack periods promote the deposition of fine-grained sediment.

Tidal amplitude attenuation in an estuary occurs from energy losses due to turbulent mixing and from frictional affects due to interactions with the bottom and lateral boundaries of the estuary. Energy dissipation of the tidal wave can be described in terms of amplitude decay of the dominant tidal constituent, which for the Gulf of Maine is the semidiurnal M2 tide that contributes about 90% of the predicted tidal variance. Not all energy is dissipated due to frictional effects, and some is transferred to higher harmonics (overtides; *e.g.*, the M4 and M6 tidal constituents) through nonlinear interactions and frictional effects that create tidal asymmetry (Aubrey and Speer, 1985; Speer and Aubrey, 1985; Parker, 1991). A comparison of the magnitude of the M2 constituent with the first harmonic M4 is a direct measure of nonlinear interactions of the M2 tide, whereas the phase difference qualitatively describes the tidal asymmetries in the system (Friedrichs and Aubrey,

* Corresponding author.
E-mail address: sc10@wildcats.unh.edu (S.E. Cook).

https://doi.org/10.1016/j.ocemod.2019.02.009
Received 25 May 2018; Received in revised form 31 December 2018; Accepted 14 February 2019
Available online 20 February 2019
1463-5003/

1988). Generation of the M6 component is largely attributed to frictional affects (Parker, 1991).

The dissipation problem is complicated by the highly nonlinear nature of tidal shoaling and propagation, and the need to define representative bottom boundary conditions that characterize the interactions between tidal currents and the seabed. Dissipation in inlets and estuaries leads to development of local phase lags between pressure and velocities that shift slack tide periods up to a quarter of the wave period (90 deg phase shifts between sea surface elevation and along channel velocity), and also impacts the evolution of tidal harmonics that are amplified and phase-shifted relative to open ocean values. This behavior can affect the overall transport in the estuary, thus a good understanding of the spatial and temporal patterns in tidal dissipation can aid in long-term coastal management and planning, for example site selection for tidal renewable energy projects (Neill et al., 2014).

The tides may also interact nonlinearly with river flow, storm surges and wind driven currents that vary on time scales of hours to months. Often observations from only a few locations are used to describe the overall dynamics of an estuary, and field experiments are limited to one specific area for a discrete amount of time. It is often not feasible to collect enough measurements continuously everywhere to adequately characterize the tides and associated flows; thus, numerical models can be used to produce system-wide predictions of water levels and currents under different hydrodynamic and meteorological forcing conditions (*e.g.*, Warner et al., 2005a). Quantitative prediction of tidal amplitudes and currents is needed for flooding and inundation studies, mooring and berthing design, safe navigation, interaction with structures, and bottom shear stress prediction for sediment transport, organism transport and nutrient fluxes.

In this study, we discuss the implementation and validation of a three-dimensional high-resolution hydrodynamic model of a tidally dominated well-mixed estuary located within the Gulf of Maine. The Gulf of Maine has a natural resonance close to the semidiurnal (M2) tidal constituent (Garrett, 1972), enhancing the tides throughout the gulf, including connected estuaries and coastal embayments including the Bay of Fundy. In this study we examine the Piscataqua River - Great Bay estuary located within the Gulf of Maine at the border of New Hampshire and Maine (Fig. 1). Tidal forcing for the Great Bay is dominated by the semidiurnal (M2) component of the tide, has a tide range on the order of 2–4 m (depending on the spring-neap cycle), and has variable (but mostly minor) freshwater river discharge. It is home to both the second deepest U.S. naval port, and Portsmouth Harbor, which is home to some of the fastest tidal currents of any commercial port on the U.S. East Coast. The estuary has two tidal regimes: a high dissipative region through the lower Piscataqua River from the mouth to Dover Point, and a low dissipative regime from Dover Pt. through the Little Bay and Great Bay (Brown and Trask, 1980; Swift and Brown, 1983). The former region behaves like a partially progressive wave with concomitant phase shift of the slack tidal period, whereas the latter has phase shifts consistent with standing waves. This behavior causes changes in the timing of tidal currents and the associated net sediment transport throughout the estuary. Previous modeling studies of the Great Bay (Ip et al., 1998; Erturk et al., 2002; McLaughlin et al., 2003) considered depth-integrated, two dimensional flow fields, with the primary focus of representing the gross tidal behavior to estimate the net transport of water and sediment in the estuary.

The model validation process includes examination of the nonlinear tidal behavior that drives tidal asymmetry and tidal energy dissipation in terms of amplitude decay and phase lags using water level measurements and harmonic analysis. Modeled results are compared with coincident and previous observations, and with results from the literature. This study will form the basis for additional modeling aimed at

Fig. 1. Site location of the Great Bay Estuary and Piscataqua River in southwestern New Hampshire, USA, relative to the Gulf of Maine (inset). The location of the 8 principal rivers of the estuary are indicated, as well as Fort Pt. (the location of a NOAA tide gauge), Dover Pt. (at the entrance to the Little Bay), and Adams Pt. (at the entrance to the Great Bay).

examining the spatial variation in bottom shear stresses needed for sediment transport calculations, horizontal and vertical mixing within the estuary, and transport of larvae, nutrients and carbon within the estuary.

Section 2 describes the field site, observational datasets, the hydrodynamic model and grid development, and the model validation and tidal analysis methodology. Section 3 describes model results, and Section 4 discusses the model-observation comparison in terms of nonlinear evolution. Section 5 presents the conclusions of the study.

2. Methods

2.1. Site description

The Great Bay Estuarine system is located along the New Hampshire-Maine border within the Gulf of Maine in the northeastern portion of the United States (Fig. 1). It is a recessed, drowned river valley connected to the Gulf of Maine *via* the Piscataqua River (Armstrong et al., 1976). The tide range is 2–4 m over the spring-neap cycle with tidal currents greater than 2 m/s in the channels at maximum ebb and flood tides. At low tide as much as 50% of the Great Bay is exposed as low-lying mudflats, cut with deep tidal channels. The surface area of the estuary is approximately 55 km^2 measured at mean high water (NHDES, 2007). The volume is $156{\cdot}10^6\ m^3$ and $235{\cdot}10^6\ m^3$ for low and high tides respectively, with a tidal prism of $79{\cdot}10^6\ m^3$ (Swift and Brown, 1983; NHDES, 2007). Seven tributaries contribute fresh water to the system: the Squamscott, Lamprey, Winnicut, Oyster, Bellamy, Cocheco, and Salmon Falls, all feeding the Upper and Lower Piscataqua river that flows into the Gulf of Maine. River fluxes are determined by precipitation and runoff and regulated by dams or weirs that modulate the freshwater volume entering the system. Typically (except during large storms or the spring melt), the freshwater input is relatively small and only contributes 2% of the tidal prism (Short, 1992; NHDES, 2007). The generally small freshwater fluxes and strong tidal mixing results in weak or negligible stratification (except very close to the river mouths) and during periods of little rainfall the salinities at the Great Bay Buoy (Fig. 3) are nearly equal to the Gulf of Maine indicating that horizontal variation in density due to river fluxes are also weak. As our interests include the ability of the numerical model to represent the vertically varying flow fields, we will include model runs with and without average river discharges to evaluate the influence of baroclinic flows on the tidal behavior.

Ocean waves outside the mouth of the estuary are strongly refracted away from the deep center channel and rapidly attenuate upstream, and thus do not greatly contribute to the velocities or water level fluctuations in the estuary, other studies have shown that waves can have an impact on tidal currents (*e.g.*, Lewis et al., 2014). Wind-driven surface gravity waves in the large lobe of the Great Bay proper are generally small (5–20 cm significant heights) owing to the limited fetch and strong attenuation by energy loss through interactions with tidal currents and the muddy bottom or shallow aquatic vegetation (eel grass meadows). Although waves on the Great Bay could be important to bottom shear stresses over the mud flats, they do not substantially alter the larger scale circulation, and thus are not considered further in this study. Wind-driven mean currents may be substantial during storm conditions, but are generally much weaker than the tidal currents (Wengrove et al., 2015) and thus are also not considered in this study.

The bathymetry of the estuary is complex (Fig. 2), with steep sidewalls in the main channel of the Piscataqua River with water depths ranging 13–26 m. Ocean water flows into mouth of the Piscataqua River through two channels, a main entry point to the north of New Castle Island between New Hampshire and Maine, and a secondary entry point through Little Harbor to the south of New Castle. Tides entering Little Harbor flow through relatively shallow water and around several islands, and join the Piscataqua River between Pierce Island and Portsmouth, NH. Flows through the main channel make a sharp 90 deg turn around New Castle at Fort Point, and then flow around the Portsmouth Naval Shipyard primarily to the south in the deeper channel but also the back bay, a narrow, shallow waterway that reconnects with the Piscataqua River near Pierce Island. The Piscataqua River splits at Dover Pt., with the main flows sharply turning south into Little Bay, and with a smaller portion of the flow heading to the north connecting the

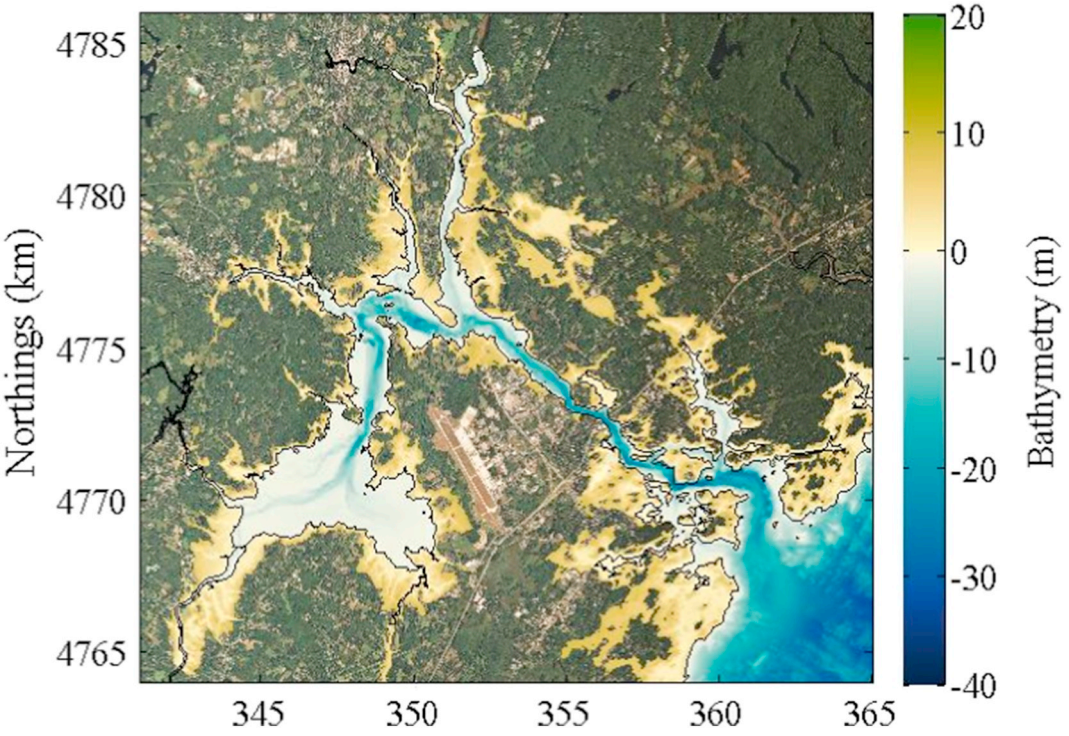

Fig. 2. Topographic and bathymetric elevations relative to mean sea level for the Great Bay Estuary. Background image is from Landsat 8.

lower Piscataqua River with the Upper Piscataqua fed by the Cocheco, and Salmon Falls rivers to the north, with average summer discharge rates of 8.54 and 15.4 m^3/s, respectively (NHDES, 2007).

The channel between the mouth at New Castle Island and Dover Pt. is 12 km long and characterized by a hard rocky bottom with coarse sediment in the deep channels and steep rocky shorelines for most of the reach. The flows through this part of the estuary are high (exceeding 2 m/s in some locations) on both the flood and ebb tides. Once the flow enters the Little Bay it remains strong through the deep center channels with weaker flows up and over the bordering mud flats. The Oyster and Bellamy rivers that flow into the Little Bay have average summer discharges of 0.94 and 1.32 m^3/s, respectively (NHDES, 2007). The Little Bay joins the Great Bay at Furber Strait near Adam's Pt. The deep center channel gradually shallows and bifurcates into an eastern and western branch flanked by large mud flats that dominate this portion of the estuary. The Squamscott, Lamprey, and Winnicut rivers all flow into this part of the estuary, with average summer discharge rates of 5.3, 10.0, and 0.7 m^3/s, respectively (NHDES, 2007). For this study, the tidal analysis focuses on the main channel flows from the mouth of the Piscataqua River to the upper reaches (Squamscott River) of the Great Bay estuary (Fig. 1).

2.2. Observations

Field observations of horizontal currents spanning the water column and sea surface elevation (from bottom pressure and tidal stations) were obtained during several field experiments in 1975, 2007, 2009, 2015, and 2016, and the continuously operating NOAA Tide Gauge station at Fort Point, NH (Station ID: 8423898). Table 1 summarizes the dates and durations of the field studies and Fig. 3 shows the instrument locations.

Observations of tidal elevations and currents within the estuary were obtained in 1975 by the University of New Hampshire (UNH) in cooperation with the National Ocean Survey (NOS; summarized in Swenson et al., 1977 and Silver and Brown, 1979). Original data were unavailable so tidal analysis estimating M2 tidal amplitudes and phases from Swift and Brown (1983) is used in this study. Observations of bi-directional currents (in 0.5–1.0 m range bins) and water levels from the mouth to Adams Pt. were obtained by NOAA in 2007 using six bottom-mounted, upward-looking acoustic Doppler current profilers (ADCPs). The instruments were deployed for between 41 and 45 days, recovered, and then moved to new locations with water depths ranging between 4.3 and 19.3 m. These data are available and described online at https://tidesandcurrents.noaa.gov. Observations of water levels were obtained by UNH in 2009 at four locations in the Great Bay using bottom mounted pressure sensors and an RTK GPS buoy. The instruments were sampled between 30 and 120 s and deployed between 9 and 84 days, and averaged over 6 min intervals following standard NOAA procedures. Observations obtained for 7–71 days by UNH in 2015 and 2016 include 1 min averaged bi-directional currents (in 0.25–1.0 m range bins) and water levels from six ADCPs deployed across the Great Bay in water depths ranging 3–17 m. Bottom pressure was converted to sea surface elevation using observed bottom temperature at the instrument location and salinity obtained from the Great Bay Coastal Buoy located in the center of the Great Bay Estuary (http://www.opal.sr.unh.edu/data/buoys/great_bay/index.shtml).

2.3. Hydrodynamic model

The Regional Ocean Modeling System (ROMS, Haidvogel et al., 2008; Shchepetkin and McWilliams, 2005) is an ortho-curvilinear three-dimensional numerical coastal ocean circulation model that solves finite-difference approximations of the Reynolds-averaged Navier Stokes (RANS) equations using the hydrostatic and Boussinesq assumptions. The objectives of this study focus on the hydrodynamic component to determine the tidal dynamics, which are of first order concern in validating the numerical model. ROMS has been used in both regional (*e.g.,* Zhang et al., 2009; Yang et al., 2016) and estuarine modeling studies (*e.g.,* Warner et al., 2005a; Moriarty et al., 2014), and implemented into other coupled modeling systems (*e.g.*, Warner et al., 2008; Warner et al., 2010).

A third order upwind advection scheme is used to solve for horizontal advection. A centered-fourth order advection scheme is used to solve for vertical advection. A k-ε generic length scale (GLS) turbulence

Table 1
Observations used in the study with number of locations and duration of deployments.

Year – program	Data variable	Number of locations	Duration
1975 – Great Bay Estuary Field Program (Swenson et al., 1977, Silver and Brown, 1979)	Water level[a,b]	10*	21–333 days
2007 – Piscataqua River Current Survey (https://tidesandcurrents.noaa.gov/cdata)	Water level and currents[c,d]	10	41–45 days
2009 – CCOM Great Bay Survey	Water level[e,f]	6	9–84 days
2015 – Great Bay Field Study	Water level and currents[g,h,i,j]	8+	7–35 days
2016 – Great Bay Field Study	Water level and currents[d]	1	71 days
NOAA Tide Gauge (8423898) at Ft. Point (https://tidesandcurrents.noaa.gov/stationhome.html?id=8423898)	Water level[k]	1	Continuous
2009–2016 – UNH Great Bay Buoy (http://www.opal.sr.unh.edu/data/buoys/great_bay/index.shtml)	Salinity[l]	1	Seasonal (~9 months)

* Original data unavailable; water levels and current analysis used in this study are provided in Swift and Brown (1983).
\+ One instrument was moved to 4 different locations within Great Bay for deployments between 7 and 14 days.
[a] Automatic digital recording (ADR) tide gauge.
[b] Metritape Inc. Level sensor.
[c] 600 kHz RDI ADCP.
[d] 1200 kHz RDI ADCP.
[e] Aanderaa tide gauge.
[f] SeaBird Seacat.
[g] 500 kHz RDI Sentinel V ADCP.
[h] 1200 kHz RDI Workhorse Sentinel ADCP.
[i] 3 mHz Sontek Arganaut ADCP.
[j] 2 mHz Nortek Aquapro ADCP.
[k] Acoustic water level (Next Generation Water Level Measurement System).
[l] YSI 6600 Sonde.

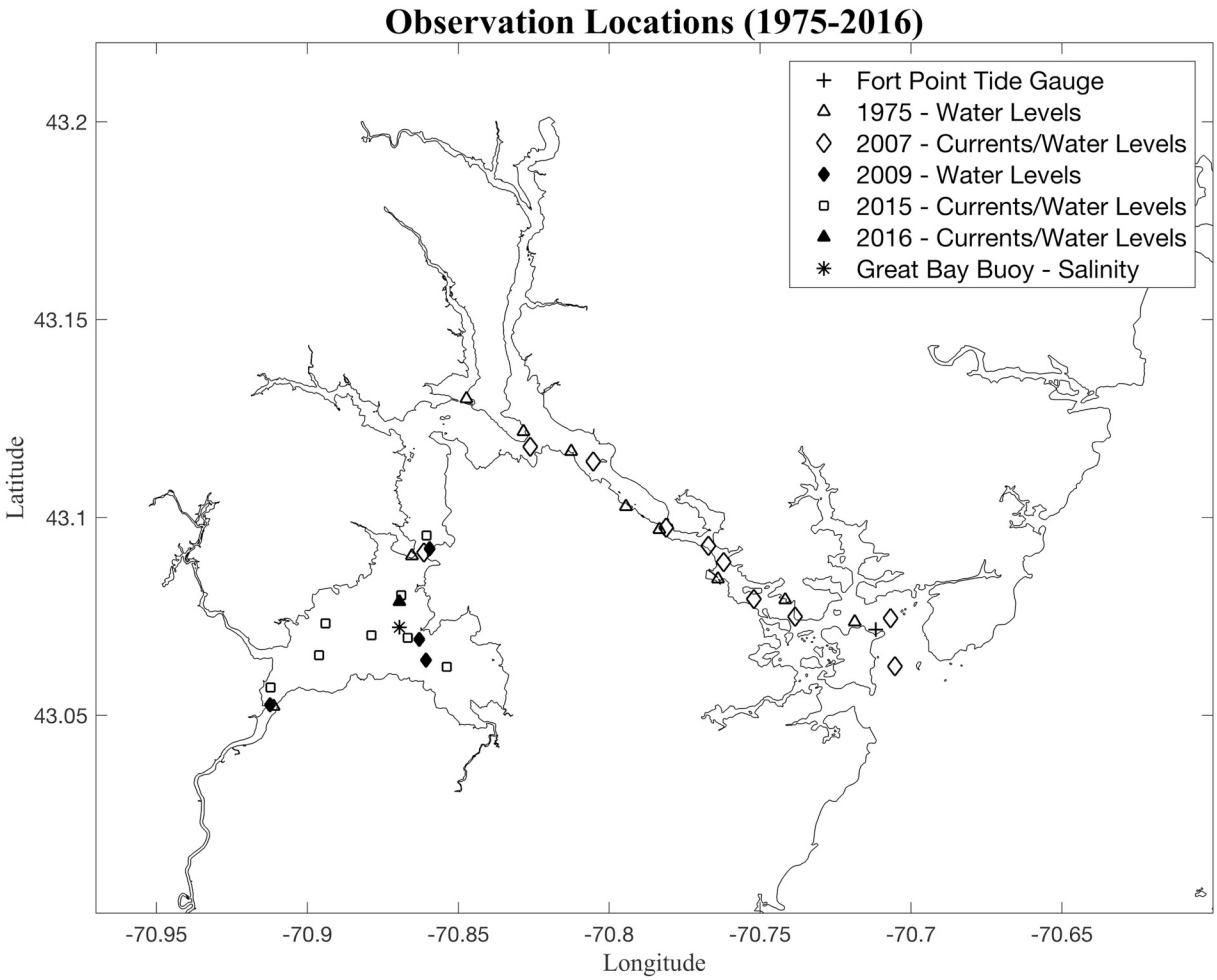

Fig. 3. Observational measurement locations. Along-channel distance from the mouth of the estuary is determined using the PIR0701 sensor (most seaward diamond symbol) from the 2007 NOAA Piscataqua River Current Survey.

closure model is used to calculate the horizontal and vertical eddy viscosities (Umlauf and Burchard, 2003; Warner et al., 2005b) in conjunction with the Kantha and Clayson (1994) stability function. Within ROMS the wetting and drying algorithm (Warner et al., 2013) is utilized to simulate the inundation and draining of the tide over shallow areas alternatively covered and uncovered by the tide, in which the critical depth (D_{crit}) is set to 10 *cm*. Once the total water depth is less than D_{crit}, no flux is allowed out of that cell and it is considered "dry". Finally, barotropic and baroclinic modes are solved separately in ROMS with the mode-splitting algorithms described in Haidvogel et al. (2008). Barotropic time steps in model simulations herein are 1/20 of the baroclinic time step.

2.3.1. Model grid

The model domain is defined by a rectilinear Arakawa "C" grid with a constant 30-by-30 *m* horizontal resolution (Fig. 4; downsized by a factor of 33 1/3 in the figure). There are 8 vertical layers in a terrain-following (σ) coordinate system that is adjusted for slightly higher resolution near the surface and bottom boundaries. The domain is rotated 37 deg CCW from true north to align the offshore boundary with the approximate orientation of the shoreline along the New Hampshire-Maine coast. The domain ranges 22.02 by 25.02 *km* (734 by 834 cells). The grid elevations were defined using bathymetric data obtained from the Center for Coastal and Ocean Mapping (CCOM; http://ccom.unh.edu), and LIDAR data collected by USGS, NOAA, and USACE (https://coast.noaa.gov/dataviewer), and interpolated onto the center of the horizontal grid cells. A hierarchy was defined that weighted the most accurate, recent, and complete topographic and bathymetric data highest, with any gaps filled with more uncertain, older, or less complete data sources. The combined elevation grid (Fig. 4) was then processed with the MATLAB Easygrid routine (https://www.myroms.org/wiki/easygrid) to create the rectilinear grid and corresponding land mask that was subsequently input into ROMS. During model testing, the grid was smoothed in locations sensitive to numerical instabilities using interpolation methods described in Plant et al. (2002).

2.3.2. Boundary conditions

At the open ocean boundary (south edge of the rotated domain; Fig. 4) the model is forced by tidal and subtidal oscillations (see Section 2.3.3) using the implicit Chapman (free surface) and Flather (depth averaged velocity) boundary conditions. The Chapman-Flather conditions employ the radiation method at the boundary, assuming all outgoing signals leave at the shallow water wave speed (Flather, 1976; Chapman, 1985). These particular boundary conditions have been shown to be the most suitable for tidal forcing (Palma and Matano, 1998, 2000; Marchesiello et al., 2001; Carter and Merrifield, 2007). Three-dimensional baroclinic momentum equations were set to radiation and gradient conditions for velocities and tracers. The eastern, northern, and western edges of the domain are closed.

The bottom boundary condition for momentum was parameterized by a simple drag coefficient assuming a logarithmic vertical velocity

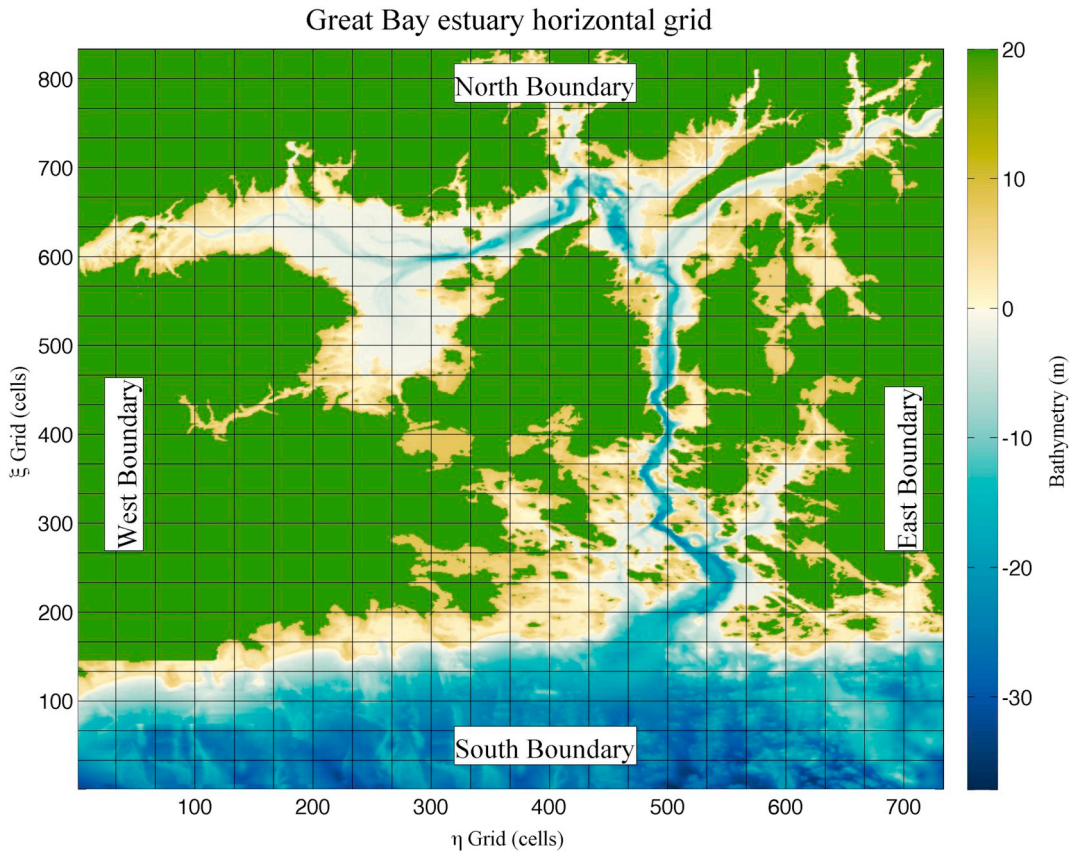

Fig. 4. Rotated ROMS horizontal grid (ξ, η) coordinates and model defined boundaries. Displayed gridlines are every 1 *km*, decimated by a factor of $33\,^{1}/_{3}$ from actual model grid (for display purposes). Cardinal directions of boundaries are relative to the orientation of the rotated grid.

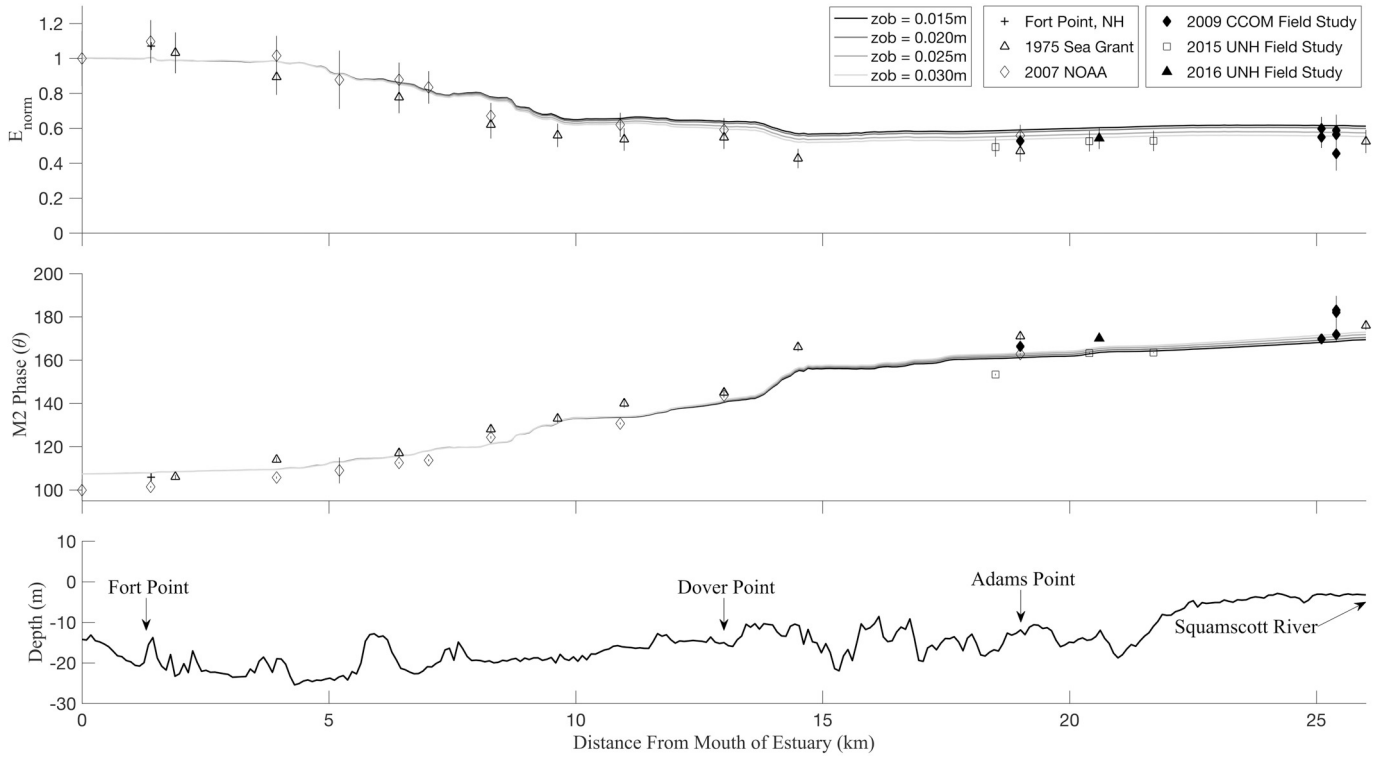

Fig. 5. M2 tidal energy decay, E_{norm}, (upper panel) and phase evolution (deg Greenwich; middle panel) as a function of distance from the mouth of the estuary for different bottom roughness values (z_{ob}) of the logarithmic drag law bottom boundary condition. Observations are included as symbols with error bars based on T_TIDE analysis and following Taylor (1982). Depth profile along the center channel is shown in the lower panel with locations of Fort Point, Dover Point, Adams Point, and the Squamscott River are indicated.

profile in the bottom vertical cell. The drag coefficient, C_D, is represented by.

$$C_D = \left(\frac{\kappa}{\ln(z/Z_{ob})} \right)^2 \quad (1)$$

where z is the vertical elevation of the mid-point of the bottom cell, z_{ob} is a characteristic bottom roughness (in m), and $\kappa = 0.41$ is the von Karman coefficient (Kundu, 1990). A range of bottom roughness values (from 0.015 to 0.030 m) were tested and the best fit was determined iteratively from model-data comparisons of M2 tidal dissipation as a function of distance from the estuary mouth (see Fig. 5). Within each run, z_{ob} was assumed to be spatially uniform across the domain. The kinematic bottom stress boundary conditions are given by.

$$\tau_b^x = \rho_0 C_D u \sqrt{u^2 + v^2} \quad (2)$$

$$\tau_b^y = \rho_0 C_D u \sqrt{u^2 + v^2} \quad (3)$$

where ${\tau_b}^x$ and ${\tau_b}^y$ are the bottom stresses in the x and y directions, respectively.

2.3.3. Model initialization and forcing

Forcing conditions at the open ocean boundary are specified in two ways. The first is with an analytical representation of tidal elevations and velocities considering only the principal semidiurnal (M2, N2, S2) and diurnal (O1, K1) tidal constituents determined by the Oregon State University global Tidal Prediction Software package (OTPS) in conjunction with the United States East Coast regional Tidal Solution (EC2010; Egbert and Erofeeva, 2002). The OTPS provided the necessary tidal amplitude and phases that correspond to the observational datasets for the 2015 field study used in the model-data comparisons of velocities (see Section 2.4.2 and Fig. 6). The amplitudes and phases compared favorably with a harmonic analysis of observed water level fluctuations at Fort Pt. for the 2015 field experiment using T_TIDE (Pawlowicz et al., 2002).

The second forcing consists of the analytical representation of the tides and including subtidal oscillations associated with atmospheric motions obtained from low-pass filtered (with a 33 hr cut-off period) observed time series of 6-minute averaged water levels at the Fort Pt. tidal station. The subtidal motions can have amplitudes in the Gulf of Maine of 0.10–0.30 m (Brown and Irish, 1992), change the water depth over the shallow mudflats considerably, and although the time scales of the oscillations are generally much longer than the dominant semidiurnal tides, may contribute to the overall water velocities on the flood and ebb. Coastal ocean currents associated with barometric, wind-driven, or other shelf motions at the offshore open boundary are assumed small (consistent with observations of currents from 2007 at the most seaward instrument location, PIR0701) and not considered herein.

In each case (tidal with or without subtidal forcing), time series of water level fluctuations are ramped hyperbolically from rest over a 2-day period. Although tidal currents are included at the open boundary, test simulations in which the boundary currents were set to zero and allowed to evolve with the sea surface fluctuations did not alter the results, suggesting that approximating the forcing by only the pressure gradient at the mouth is reasonable (consistent with Geyer and MacCready, 2014). Time series of at least 32 days are used to force the model so that tidal analysis with T_TIDE produces amplitudes and phases of the dominant tidal constituents (with confidence intervals). The open ocean boundary is located about 7.5 km from the mouth of the estuary where the Fort Pt. tide station is located. The time for the tide wave to propagate this distance is small, about 7.3–8.1 min based on an average water depth of 30–24 m, and thus has small effect on the phase estimates (about 3.3–3.9 deg) when comparing to coincident observations within the estuary.

Three-dimensional simulations were performed both with and without freshwater flows based on the average summer river discharge (see Section 2.1), salinity (varying between 6.93 and 23.54 psu), and water temperature (varying between 19.5 and 25.4 $deg.\ C$) for the various rivers for the summer of 2015 was provided by the New Hampshire Department of Environmental Services (https://www.des.nh.gov/organization/divisions/water/wmb/vrap/data.htm). Ocean water temperature (17 $deg.\ C$) and salinity (31.5 psu) was assumed constant and given by typical summer values for the Gulf of Maine. Diurnal surface heating and cooling were assumed small in comparison to the tidal mixing and were ignored. Although the precise values of the fluctuating river discharge, temperature, and salinity were not used in the model, the variations in temperature and salinity predicted by the model compare favorably with 2015 observations obtained in the middle of the Great Bay near the surface with the Great Bay Coastal Buoy (http://www.opal.sr.unh.edu/data/buoys/great_bay/index.shtml) and near the bottom with the SeaBird instruments co-located with our ADCP's deployed in 2015. Modeled and observed fluctuations in temperature and salinity follow tidal cycles and reveal weak vertical gradients in temperature (about 1–2 $deg.\ C$) and salinity (about 1–2 psu), consistent with a well-mixed Great Bay environment away from the river mouths during typical summer conditions in New Hampshire.

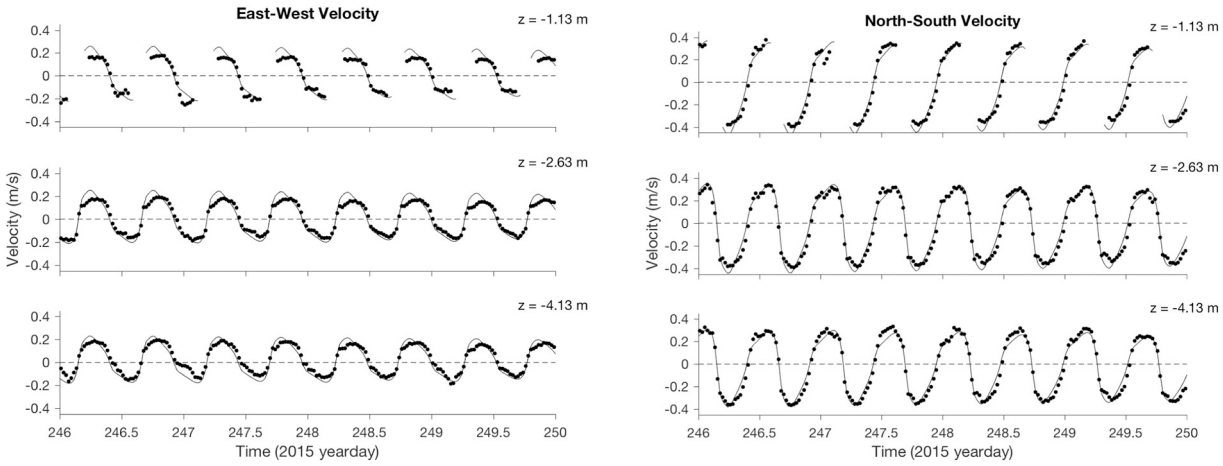

Fig. 6. Modeled (dots) and observed (solid line) time series of east-west (left) and north-south (right) velocities from sensor located in 5.75 m water depth in the Great Bay. The vertical elevation relative to mean sea level (in m) of each time series comparison is indicated on the right-hand-side of each panel. The discontinuous time series in the upper three panels are a result of tidal variations in water depth periodically exposing and inundating upper sensor locations near the sea surface. RMS errors range 0.035–0.049 m/s and 0.047–0.055 m/s for the east-west and north-south velocities, respectively.

Model simulations including subtidal oscillations and river fluxes had a very weak effect on the tidal behavior and thus the results presented below will focus on the model simulations for barotropic tides. This is not unexpected for the typical summer conditions examined herein, but might be an important consideration during extreme storms and high runoff periods or in the very shallow depths near the water's edge over the mudflats. The effect of subtidal oscillations and baroclinic flows is discussed further in Section 4. In the following, tidal analysis from model simulations will be compared with observations within the estuary obtained in different experiments at different time periods (tidal constituents are assumed to be the same throughout). Our model runs focus on the 35 day period spanning the 2015 field experiment, and will be compared with observed velocity and sea surface elevation time series from 2015 and tidal analysis of observations obtained during all experimental periods (Table 1).

Time resolution was determined by iteration on grid smoothing and reducing barotropic and/or baroclinic time steps until numerical stability was achieved. For model simulations presented herein, a baroclinic time step of 1.5 *s* was used, with barotropic time step 1/20 of that value. Computations were performed on a Cray XE6m-200 supercomputer at the Institute of Earth, Ocean, and Space at the University of New Hampshire, and the Blue Waters CRAY XE6 supercomputer located at the University of Illinois-Urbana-Champaign. Output over the whole domain was stored to disk at 30 *min* average model time intervals, and for 15 *min* averaged intervals at specific save points corresponding to instrument locations and along a densely sampled line every 100 *m* along the main transect passing through the entire estuary.

2.4. Model validation methods

Model validation is accomplished in four ways. The first is by conducting a tidal analysis, and comparing the modeled energy decay and phase shift of the dominant M2 tidal constituent throughout the estuary with similar analysis of observations of sea surface elevation time series. The second is by comparing modeled time series of the vertical variation in currents with observations. The third is with cross-spectral analysis between modeled and observed sea surface elevation, and horizontal velocity components at single locations, and with the evolution of cross-spectral phase at the M2 frequency between sea surface elevation and along-channel velocities. The fourth is by comparing the growth and phase change of M4 and M6 tidal harmonic constituents between modeled and observed time series, and by comparison of the along-estuary evolution of sea surface elevation skewness and asymmetry.

2.4.1. Tidal dissipation and phase change

As the tide propagates into shallow coastal regions and interacts with bottom topography and basin geometry, it loses energy through frictional processes that result in tidal amplitude decay and phase changes relative to the open ocean value. Due to phasing of the tide a direct time series comparison is only possible for model runs that coincide with the specific phases of the tide during that particular field study. However, tidal analysis of long (30+ day) time series of sea surface elevation obtained at other times can be compared with non-synchronous model simulations, provided there are no other atmospheric effects that nonlinearly interact with the tide and do not substantially change the tidal behavior. Therefore, we conduct a tidal analysis (using T_TIDE; Pawlowicz et al., 2002) to decompose each time series of sea surface elevation into tidal components and compare the modeled and observed tidal constituent energy from the linear gravity wave relation,

$$E = \frac{1}{2}\rho g A^2 \tag{4}$$

where E is the total energy per unit surface area, A is the amplitude of the tidal constituent, and the density ρ is assumed constant throughout the estuary. In this study the semidiurnal M2 tide dominates, contributing about 88% of the total tidal energy at the mouth of the estuary. The energy at any location within the estuary, $E_{station}$, is normalized by the value at the estuary mouth, E_{ocean}, to represent the fractional energy loss, E_{norm}, as the tide progresses upstream,

$$E_{norm} = (A_{station}/A_{ocean})^2 \tag{5}$$

Assuming the uncertainties in the tidal amplitudes, $\delta A_{station}$ and δA_{ocean}, are both independent and random, then the error δE_{norm} is calculated following Taylor (1982),

$$\delta \mathrm{E}_{\mathrm{norm}} = \mathrm{E}_{\mathrm{norm}} \cdot \sqrt{2 * (\delta A_{station}/A_{station})^2 + 2 * (\delta A_{ocean}/A_{ocean})^2}. \tag{6}$$

Initial model calibration involves testing different bottom boundary conditions, and iterating to estimate the energy decay as a function of distance from the estuary mouth that best fits the observations.

2.4.2. Time series comparison of vertically varying currents

Modeled currents are computed at defined σ coordinate levels that range from $\sigma = -1$ at the bottom to $\sigma = 0$ at the surface. The total water depth in the model is given by the elevation of the seabed (relative to the model datum defined) plus the corresponding (fluctuating) sea surface elevation. The observations, on the other hand, are obtained from fixed, upward looking ADCP's with vertical bin elevations defined in a fixed coordinate system relative to the bottom. The range over which the currents are observed depends on the instrument characteristics (*e.g.*, acoustic frequency and instrument capabilities) and the height of the fluctuating sea surface relative to the bottom. Acoustic interference by side-lobes at the surface limit the range of useable vertical bins to be less than 94% of the total instantaneous water depth (and appropriate filtering methods must be employed to eliminate spurious velocities near the surface). As a consequence, the velocities observed with ADCP's in the field further from the bottom have bins coming into and out of the water column as the tide rises and falls.

To compare the modeled to observed currents, the modeled currents (in σ coordinates) are transformed to the observational coordinate system by linear interpolation over the instantaneous water level at each time step. In this manner, the modeled time series at the transformed upper bins also come into and out of the water surface similar to the observations. Care must also be taken to represent the velocities from the observations at the center of the vertical bins, and the model at the defined location by the σ coordinates. A representative example of the time series comparison is shown later (Fig. 6) and described in Section 3.2.

2.4.3. Cross-spectral analysis

A more complete evaluation that includes the overall behavior of the modeled velocities can better be done with cross-spectral analysis that shows the energy density levels for both the model and the data as a function of frequency, and the coherence and phase relationship for each frequency. As our interests lie with the tidal constituents, the frequency resolution of the spectra will necessarily need to be fine enough to resolve the major constituents, with lowest tidal constituent (the O1 diurnal variation) of about $0.0417\,h^{-1}$. At the same time, the confidence intervals on the spectra, coherence, and phase must be high enough to make reasonable comparisons. For the 30 day time series examined, cross-spectra were computed with 10 degrees of freedom (DOF) by averaging 5 adjacent frequency bands. The frequency bandwidth of the smoothed spectral estimates was $0.0069\,h^{-1}$ with lowest resolved frequency of $0.0035\,h^{-1}$. The 95% confidence intervals are computed for the spectral amplitudes, coherences, and phase. Only those phase estimates for frequencies with coherence greater than the 95% critical value (0.52 for 10 DOF) are shown (phase error bars for incoherent frequencies are meaningless; Bendat and Piersol, 2000). To reduce leakage effects, a Hanning data window is applied to each mean-corrected time series before computing the spectra.

2.4.4. Sea surface elevation and along-channel velocity phase difference

Tidal analysis of the sea surface elevation and velocities can be compared to show the relative change in phase as the tide evolves up the estuary. In this case, the observed and modeled bi-directional velocities were rotated to align with the along-channel direction using standard rotary analysis (Gonella, 1972). Ellipse orientations for the dominant M2 tidal frequency define the angle of the major axis of the rotary ellipse that is used in the rotation to along-channel direction. We conduct a tidal analysis to decompose each time series of the along-channel velocity into amplitudes and phases for each harmonic tidal constituent frequency following the same procedure for the sea surface elevation (see Section 2.4.1). The phase difference between the sea surface height (P) and along-channel velocity (U) at the M2 tidal frequency was computed for time series at locations that span the estuary and reported as the $P-U$ phase.

The evolution of the $P-U$ phase for the dominant M2 tidal constituent indicates the nature of the tidal motion throughout the estuary (Fig. 10; top panel). In a progressive wave, the maximum currents occur at the same time as the maximum height of the wave, and the currents and amplitude are in phase. In a standing wave the maximum currents occur at mid-tide, half way between the crest and the trough of the wave, and the along-channel currents are 90 deg out of phase with the sea surface height.

2.4.5. Tidal harmonic growth and phase difference

The growth of the M4 harmonic relative to the M2 constituent is a measure of the asymmetry and non-linear distortion of the tide (Friedrichs and Aubrey, 1988). Following Speer and Aubrey (1985), the amplitude ratio, A_{ratio}, and the phase difference, θ_{diff}, is defined as,

$$A_{ratio} = A_{\mathrm{M4}}/A_{\mathrm{M2}} \tag{7}$$

$$\theta_{diff} = 2 * \theta_{\mathrm{M2}} - \theta_{\mathrm{M4}} \tag{8}$$

where A_{M4} and A_{M2} are the amplitudes of the M4 and M2 tidal constituents, respectively, and θ_{M4} and θ_{M2} represent corresponding phase relationships. In general, stronger frictional effects produce larger A_{ratio}, and the corresponding θ_{diff} describes the gross behavior of the tides with phase differences between 0° and 180° (180° and 360°) indicating flood (ebb) dominance (Friedrichs and Aubrey, 1988). Flood dominant systems have characteristically stronger flood currents and longer falling than rising tides, whereas ebb dominant systems have stronger ebb currents and longer rising tides.

The amplitudes and phases of the M2 and M4 tidal constituents are estimated with a tidal harmonic analysis (using T_TIDE) that fits harmonics to the time series and computes error bars on the estimates of amplitude and phases for each constituent, allowing estimates of the uncertainty in A_{ratio} and θ_{diff} (Taylor, 1982). The error estimates for δA_{ratio} and $\delta\theta_{diff}$ are calculated using the following formulations,

$$\delta \mathrm{A}_{\mathrm{ratio}} = \delta \mathrm{A}_{\mathrm{ratio}} \cdot \sqrt{(\delta A_{M4}/A_{M4})^2 + (\delta A_{M2}/A_{M2})^2} \tag{9}$$

$$\delta\theta_{diff} = \sqrt{(\delta\theta_{\mathrm{M2}})^2 + (\delta\theta_{\mathrm{M4}})^2} \tag{10}$$

following Taylor (1982), similar to δE_{norm} (Eq. (6)).

The third moments, skewness and asymmetry, of observed and modeled sea surface elevation time series are computed along the estuary (following Elgar and Guza, 1985). The normalized (by the variance to the 3/2 power) skewness describes the general nonlinear deviation of the wave profile from a sinusoidal shape to a peaked-up waveform symmetrical about the vertical axis through the wave crest. The normalized asymmetry describes the asymmetry about the vertical axis, and can indicate a pitched forward (or pitched backwards) wave form. The nature of the skewness and asymmetry is determined by the phase relationship between the primary frequency and the coupled harmonics. For purely skewed (peaked up, Stokes-like) wave profiles, the asymmetry is zero and the primary and higher harmonics are in-phase. For pitched forward (backward) the asymmetry is nonzero and negative (positive). Sawtooth profiles have high negative asymmetries and phase relationships between the primary and first harmonic up to ± 90 deg. Evaluation of waveforms for wind-driven surface gravity waves in the ocean and their relationship to third moments can be found in Elgar and Guza (1985).

3. Results: model-observation comparison

Results comparing model simulations for barotropic tides with observations are presented here, and follow the methodologies discussed previously. Station data are retained from the model simulations at all the sensor locations, as well as from locations separated by 100 m along a transect down the main channel extending from the first sensor location outside the mouth of the estuary to the upper reaches of the Great Bay by the Squamscott River.

3.1. Tidal dissipation and phase change

The observed energy decay and phase change of the M2 tidal constituent relative to the value at the most seaward location along the station transect through the estuary is shown in Fig. 5. The most seaward observation (1 km from the Ft. Point tidal station) closely matches the predicted tidal amplitude from the OTPS model, and used to normalize the energy (E_{norm}, Eq. (5)). Also shown is the variation in the center channel water depth along the transect. Error bars (Eqs. (5)–(6)) on the energy and phase estimates are based on the T_TIDE analysis. Observations show an increase in tidal energy near the mouth, and then a progressive decrease in energy through the energetic, narrow portion of the lower Piscataqua River. This decay is strong (and somewhat variable) between Portsmouth and Dover Pt., and in general agreement with estimates of dissipation found by Swift and Brown (1983). By the time the tides reach the Little Bay entrance, 45% of the M2 tidal energy has been lost. Over this same reach, the M2 phase has changed 50 deg, significantly larger than for a simple progressive tidal wave propagating upstream (with estimate of about 6 deg phase change based on shallow water wave phase speeds and average water depth of 20 m), and much less than a standing wave with 90 deg phase change.

Interestingly, the tidal amplitudes increase slightly between the entrance to the Little Bay (Dover Pt.) and the upper reaches of the Great Bay (Squamscott Bridge), indicating some amplification as the tide propagates into progressively shallower water. Additionally, the phase continues to evolve (approaching 70 deg) suggesting that the tide here is more reflective. It should be noted that the tidal extent during the flood does not end at the Squamscott Bridge, but continues an additional 8 km inland (as well as up the other rivers; Fig. 1).

Also shown in Fig. 5 are model predictions of the M2 tidal decay and phase change for a range of apparent bottom roughness, z_{ob}, from 0.015 to 0.030 m. The best fit to the observation is for $z_{ob} = 0.02$ m. The model increase in M2 energy across the shallowing Great Bay bathymetry is in general agreement with the observations. In general, the model well predicts the evolution of the tidal phase throughout the estuary.

3.2. Time series comparison of vertically varying currents

Comparisons of modeled and observed current time series (for 4 days) from a single location in water depth of about 5.75 m in the Great Bay is shown in Fig. 6. Both the east-west and north-south velocity comparisons are shown for elevations (relative to MSL) near the bottom (−4.13 m), mid water column (−2.63 m), and near the surface (−1.13 m). In general, the modeled velocities closely follow the observations including in the upper water column were the “sensor” bins are coming into and out of the water as the tide rises and falls. Root-mean-square (RMS) errors between modeled and observed time series at all elevations above the bottom range 0.035–0.049 m/s and 0.047–0.055 m/s for the east-west and north-south velocity components

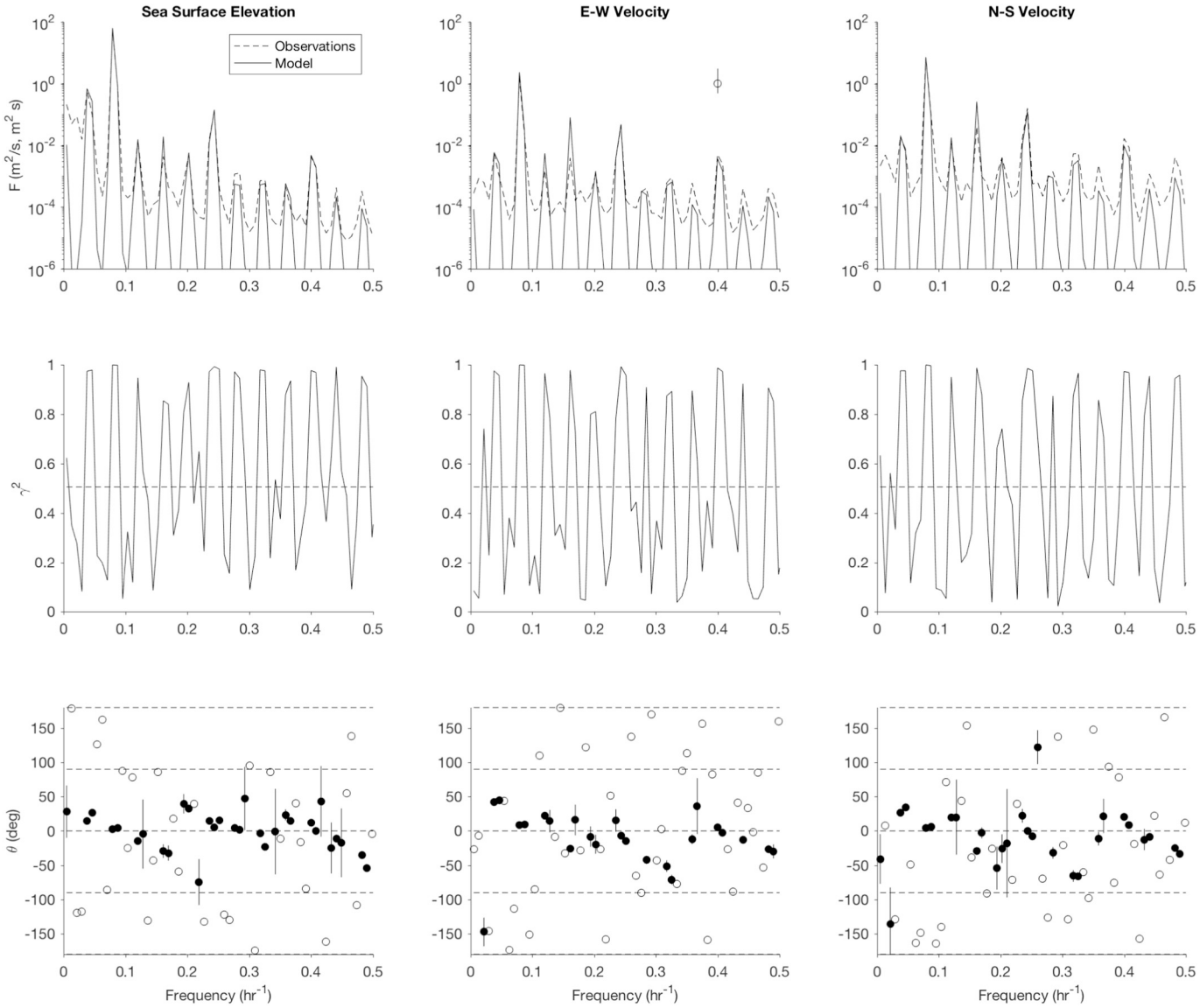

Fig. 7. Cross-spectra between modeled and observed sea surface elevation (left panels), east-west depth-averaged velocity (center panels), and north-south depth-averaged velocity (right panels) for sensor location in 5.75 *m* water depth in the Great Bay. Upper panels show spectral density, *F*, in m^2s for sea surface elevation and m^2/s for velocities as a function of frequency (hr^{-1}). Spectra were computed with a Hanning data window and 10 DOF. The 95% confidence interval is shown in the upper center panel. Observed spectra have a significantly higher noise floor but still below the energy levels of the harmonics. Center panels show the coherence squared, γ^2, with 95% significance level as the horizontal dashed line. Lower panels show the phase (*deg*) with solid circles indicating significant phases with 95% confidence intervals.

and 0.095 *m* for sea surface elevation (each about 10% of the amplitude at that location). In general, the 10% RMS error between model-data time series for all sensors across the Great Bay from the 2015 deployment is quite good, with average RMS errors for sea surface elevations, east-west, and north-south velocities of 0.096 *m*, 0.054 *m/s*, and 0.060 *m/s*, respectively.

3.3. Cross-spectral analysis

Cross-spectra between modeled and observed sea surface elevation, east-west, and north-south currents from a location in the Great Bay are shown in Fig. 7. Modeled and observed spectral density, *F*, show similar energy distribution at the tidal constituents, and compare well for the sea surface elevation and both orthogonal components of the velocity. Note that the noise floor associated with the observed spectra is much higher than for the model, a result owing to the sampling uncertainty associated with the pressure sensors and acoustic profiling instruments, as well as the model not considering baroclinic flows (discussed later).

The coherence squared, γ^2, is high (0.99) at the tidal harmonic frequencies, well above the critical value (0.52). The corresponding phase at the energetic M2 frequency is 2.47 deg for the sea surface elevation time series, and 8.48 and 3.98 *deg* for the east-west and north-south velocities, respectively. The average model-data phase at the M2 frequency for all sensors in the Great Bay during the 2015 deployment for sea surface elevation and the bi-directional velocities was 0.03, 0.34, and 2.32 *deg*, respectively.

3.4. Tidal harmonic growth and phase difference

Modeled and observed power spectra of sea surface elevation, *F*, from two locations spanning the estuary – one near the mouth at Fort Point and the other in the Great Bay – are shown in Fig. 8. The M2 tidal energy decays by about 45% (as shown in Fig. 5). On the other hand, the spectra show a sharp increase in the energy levels at the tidal

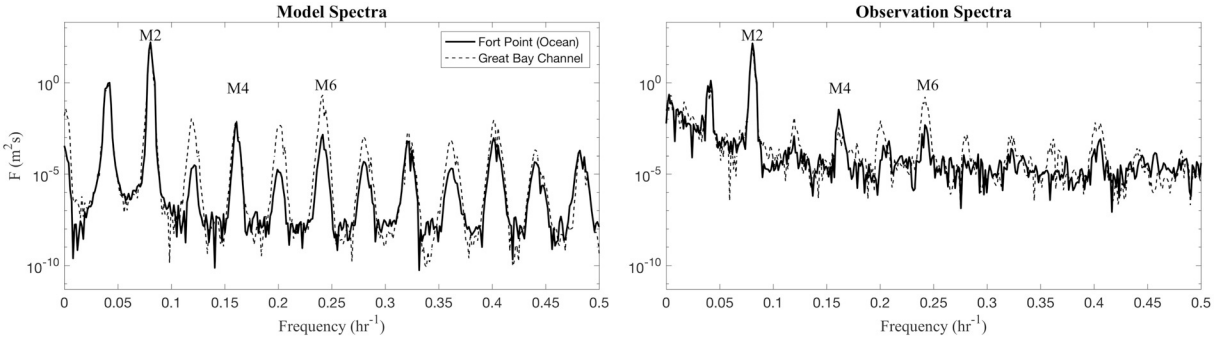

Fig. 8. Modeled (left) and observed (right) spectral density, $F\ (m^2/s)$, of sea surface elevation from two stations, one near the mouth of the estuary (Fort Point; solid line) and one in 5.75 m water depth in the Great Bay (dotted line). Spectra show the growth of the tidal harmonics from the ocean to 20 km up the estuary (the M2, M4, and M6 constituents are indicated). Spectra were computed over a 30 day record and processed with a Hanning data window. Observed spectra have a significantly higher noise floor but still below the energy levels of the harmonics.

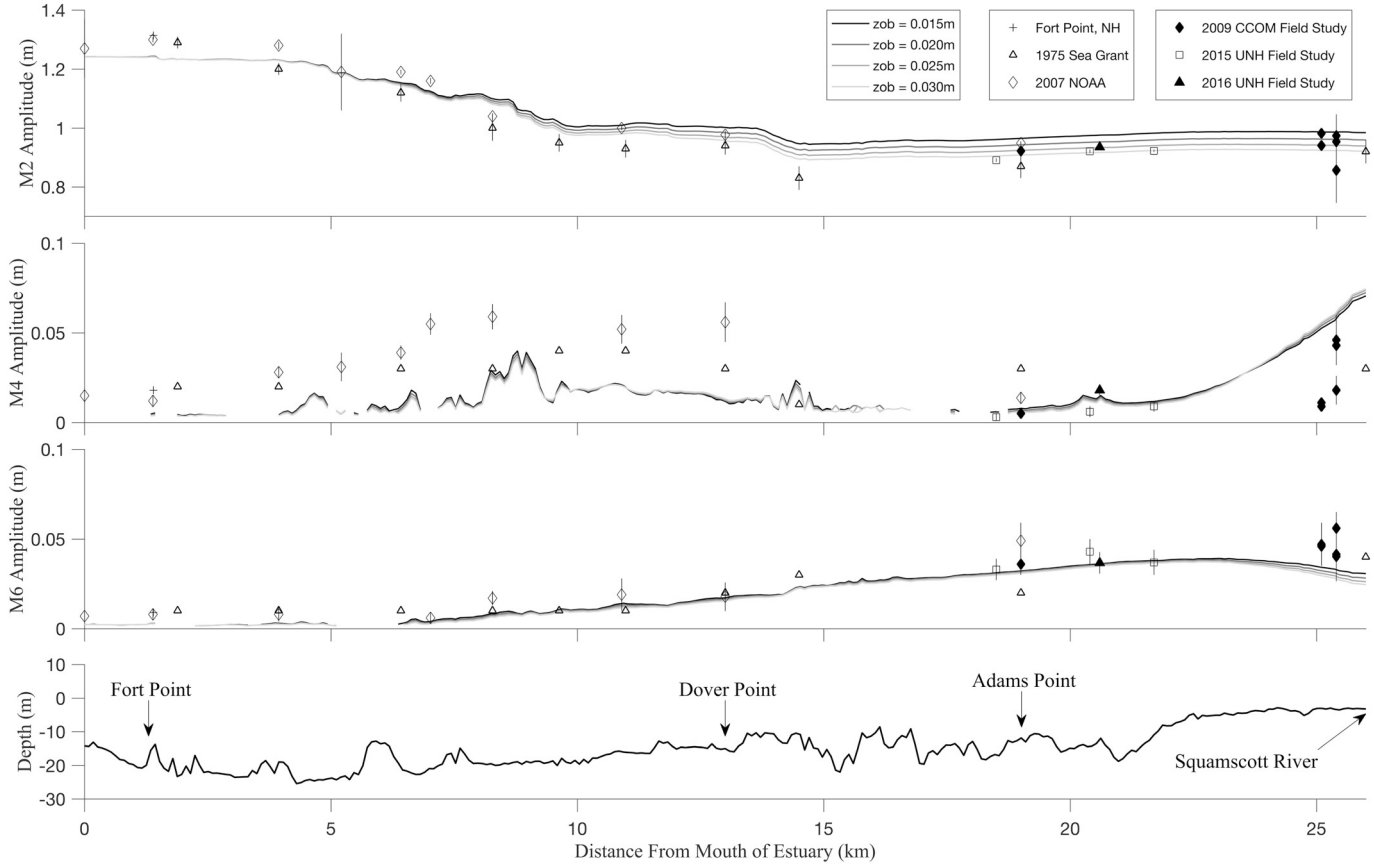

Fig. 9. Modeled (lines) and observed (symbols) amplitude evolution of the M2 (top), M4 (2nd from top), and M6 (3rd from top) tidal constituents from Fort Point, near the mouth of the estuary, to the Great Bay. Amplitudes were determined with T_TIDE analysis of 30+ day records (or for the 1975 data from the literature of which no error bars are available). Model results for a range of bottom roughness, z_{ob}, are indicated in the legend. The depth profile along the center channel is shown in the lower panel.

harmonics in the Great Bay, evident well beyond the M4 and M6 constituents indicating the strong growth of overtides and nonlinear evolution of the spectra. The growth of the M6 harmonic exceeds that of the M4 harmonic, consistent between the modeled and observed spectra.

To examine the spatial nonlinear evolution of the tidal spectra, the M2, M4, and M6 tidal constituents (as determined by T_TIDE analysis) along the center channel from the mouth to the upper reaches of the Great Bay is shown in Fig. 9 (along with the depth variation along the transect). The M2 tidal amplitude decays as expected. Modeled M4 and M6 harmonics increase from 2% to 7% of the M2 amplitude, consistent with the observations. Interestingly, the M4 amplitude first grows through the first 8 km of the Piscataqua River, then decays to very small value at Dover Pt., and then grows again in the upper reaches (last 3 km) of the Great Bay over the mudflats. The spatial evolution of the M4 tidal constituent is qualitatively similar to the observations but underestimates the magnitude by about a factor of 2 in the narrows of the lower Piscataqua River, and overestimates in the upper reaches of the Great Bay. Similar results are obtained if we include baroclinic or subtidal flows. We do not fully understand why this is occurring, but may arise from complexities in the bathymetry and sidewalls in this part of the estuary not well resolved in the model, or from viscous or

turbulent effects assumed constant throughout the model domain. Moreover, it has been shown that locally high values of the M4 tide can occur near headlands as a result of the centrifugal component of the advection of M2 momentum (Parker, 1984). Further investigation will need to address the role of bathymetric resolution and topography in the local generation of the M4 tide. The M6 tidal amplitude shows a steady increase throughout the estuary, leveling off (and even decaying near the Squamscott) over the final 3 *km* in the Great Bay. The M6 tidal constituent, driven primarily by frictional effects (Parker, 1991), appears to be well modeled throughout the estuary.

The phase evolution across the estuary is shown in Fig. 10 (top panel) for the M2 tidal frequency at all observation stations where time series are available (Table 1). The modeled evolution of the $P-U$ phase closely follows that of the observations. The $P-U$ phase relationship in the first 12 *km* of the estuary is consistently about 45° indicating a partially progressive and standing wave motion. However, 12 *km* upstream the $P-U$ phase abruptly changes to $+90$ *deg*, consistent with a standing wave from Dover Pt. through the Great Bay Estuary. This change in $P-U$ relationship is consistent with the observed tidal dissipation and relative phase change of the M2 tidal constituent (Fig. 5).

Also shown in Fig. 10 is the evolution of the growth of the M4 relative to the M2 constituent (A_{ratio}; Eq. (7)). The modeled growth of the M4 harmonic increases through the first half of the lower Piscataqua River, decreasing at Dover Pt., and then increasing again through the upper reaches of the Great Bay (to about 8% of the M2 amplitude) where the depth shallows significantly over the mudflats. The evolution of the tide depends strongly on the water depth, consistent with a nonlinearly shoaling tidal wave. This spatial behavior is qualitatively consistent with the observations that show about twice as much harmonic growth as the model in the lower Piscataqua.

Also shown in Fig. 10 is θ_{diff} (Eq. (8)), an indication of the relative importance of the ebb and flood tide to the circulation (following Friedrichs and Aubrey, 1988). Although the model under-predicts the growth of the M4 constituent, the phase differential is qualitatively consistent with the observations. The lower reaches of the estuary in the Piscataqua River show ebb dominance, consistent with a stronger receding tide as the estuary drains. The Great Bay (beyond Adam's Pt.), on the other hand, shows a strong flood dominance, indicating the flows into the bay and over the mudflats are greater than that produced by the ebb tide. This behavior is consistent with the evolution of the sea surface elevation skewness and asymmetry (Fig. 10). The skewness shows similar trend to A_{ratio} and θ_{diff}, and is relatively low through the Piscataqua river, growing in the Little Bay and Great Bay suggesting a strong nonlinear evolution to the shoaling tide wave with asymmetrical form about the horizontal (along-channel) axis. The asymmetry increases in magnitude sharply in the Great Bay, indicating a pitched forward wave profile that has shorter duration but stronger flood currents and longer duration but weaker ebb currents, consistent with the flood dominance estimated from θ_{diff}.

4. Discussion

The tidal dissipation and phase evolution in the model is modified by the choice of apparent bottom roughness, z_{ob}. A range of values for z_{ob} were introduced in model simulations and the best fit of the model tidal analysis to the observed M2 energy and phase evolution used to determine the most appropriate value. Our best estimate, $z_{ob} = 0.02\ m$, is consistent with Swift and Brown's (1983) estimates based on the 1975 observations. In their work, they find a range of frictional coefficients from 0.015 to 0.054. They also note that the dissipation was highest in regions where the flows were larger, generally occurring in parts of the estuary where there are constrictions in the flow owing to a narrowing of the river channel. Our model results show that ranges of z_{ob} from 0.015 to 0.030 *m* give reasonable results throughout the estuary, and suggest that the dissipation is well represented with a single value. This is somewhat surprising in that the character of the seafloor (ranging from rocky and coarse sediments in the channels to fine sands and muds on the flats) changes significantly over the estuary. On the other hand, the flows also change similarly. That is, where the flows are highest, the more rocky the bottom and more coarse the sediments (*i.e.*, the fine

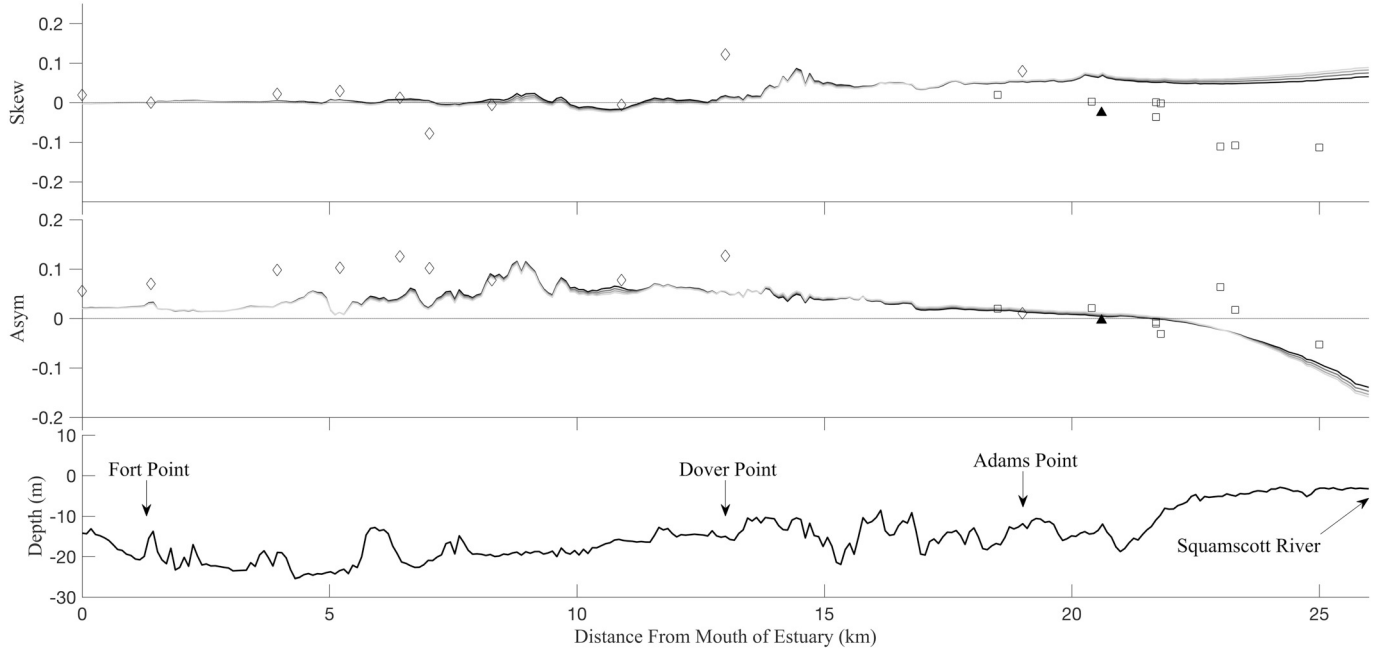

Fig. 10. Modeled (lines) and observed (symbols) along-channel evolution of the $P-U$ phase (*deg*; top panel), A_{ratio}(2nd from top), θ_{diff} (3rd from top; showing flood and ebb dominance), normalized skewness (4th from top), and normalized asymmetry (5th from top) of 30 day sea surface elevation time series from the ocean to the upper reaches of the Great Bay. The nonlinear evolution of the tide is clearly evident with the sea surface profile evolving from a partially progressive nearly sinusoidal form and ebb dominance between Fort Pt. and Dover Pt., to a nearly standing wave with highly skewed and pitched-forward shape and flood dominance in the Great Bay. Model results for a range of bottom roughness, z_{ob}, are indicated in the legend. The depth profile along the center channel is shown in the lower panel.

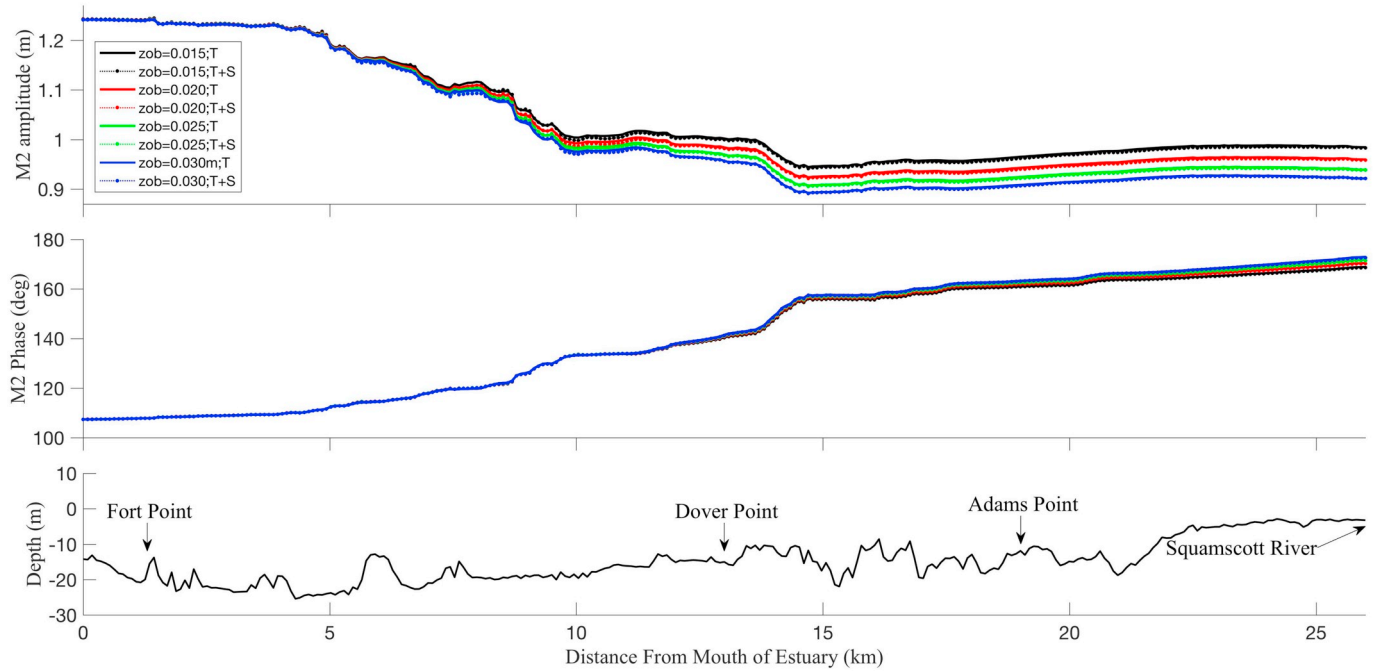

Fig. 11. Modeled amplitude evolution for tidal only (solid lines) and tidal plus subtidal forcing (symbols) for the M2 tidal constituents from Fort Point, near the mouth of the estuary, to the Great Bay. Amplitudes were determined with T_TIDE analysis of 30+ day records. Model results for a range of bottom roughness, z_{ob}, are indicated in the legend. The depth profile along the center channel is shown in the lower panel. (For interpretation of the references to color in this figure legend, the reader is referred to the web version of this article.)

material is washed away), and where the flows are weak, the more fine-grained the sediments and the nature of the bottom changes (*i.e.*, with tidal channels cut through the mud and vegetation).

Model simulations that include and exclude subtidal forcing show that the tidal dissipation (based on tidal analysis and considering only the M2 tidal constituent) does not change significantly (Fig. 11). This suggests that for the conditions examined with subtidal amplitudes ranging 0.10–0.30 m over the 30-day model runs and observation periods, the nonlinear interaction with the tides is weak. This also suggests that tidal dissipation and phase change produced from the model simulations conducted with 2015 forcing conditions can be compared with observations taken at other times (for example, from all the other experiments; Table 1).

The freshwater input to the Great Bay estuarine system is relatively small and during non-storm conditions contributes about 2% of the tidal prism (Short, 1992; NHDES, 2007). Baroclinic model simulations with average river discharge and average salinity and temperatures had a negligible effect on the tidal constituent amplitudes and phases, and can generally be ignored for the Great Bay when considering the tidal dynamics. However, comparisons of modeled time series and spectra with observations suggest that baroclinic flows are present. RMS velocity comparisons between barotropic and baroclinic model simulations away from the rivers but within the Great Bay are quite similar, and agree to within about 0.01–0.02 m/s. However, in the deep channel of the Little Bay where the flow field is high and has strong lateral shear, the baroclinic model velocities deviate from the barotropic velocities by about 0.05–0.10 m/s. Moreover, spectral comparisons show that, although the energetic tidal frequencies are not strongly affected, the high frequencies and the noise floor between the tidal harmonics increases for the baroclinic flows. This suggests that if higher frequency flows are of interest, then baroclinic models should be considered, but that tidal dynamics are well modeled with barotropic approximations.

In this work, we have not considered the effects of waves or winds on the tidal circulation and dissipation. In hindsight, this appears to be a reasonable assumption, at least for the conditions that occurred during the various field experiments. As noted by Wengrove et al. (2015), wind-generated currents during a large storm can enhance the tidal flows when the winds are in the same direction as the current. Considering that the tides reverse every 12.4 h in the Great Bay, this direct wind-driven flow might have an asymmetric effect on the overall current speeds and directions, sometimes in the direction of the flow and other times opposing or acting at an angle. In any case, the effect appears to be small even for the large wind event examined in Wengrove et al. (2015), and does not likely change the overall character of the tidal currents owing to the order of magnitude difference between the wind-induced flows (of order 0.1 m/s) and the tides (of order 1–2 m/s). This may not be true closer to shore where the tidal flows are weaker and the wind-induced currents may be proportionally larger.

The model-data comparisons show that the ROMS model reasonably well simulates the tidal dissipation and nonlinear evolution throughout the Great Bay Estuarine system. Ignoring baroclinic flow and subtidal oscillations does not strongly affect the tidal dynamics, at least for typical non-storm conditions for the Great Bay region. The model makes the hydrostatic approximation, and solves the RANS equations in three-dimensions following rectilinear horizontal grid and a vertical terrain-following σ coordinate system. Many other models (such as ADCIRC, Westerink et al., 1992; FVCOM, Chen et al., 2003; Delft3D, Lesser et al., 2004) also solve the same equations with similar approximations for rectilinear or unstructured grids and would likely also produce similar results. The good agreement between modeled and observed velocities across the estuary tidal channels and over the mud flats suggests that modeled currents from these fully nonlinear models would produce a good representation of the flow fields useful for sediment transport and nutrient flux studies (the subject of ongoing work).

5. Conclusions

A high-resolution three-dimensional hydrodynamic model (ROMS) was implemented for the Piscataqua River - Great Bay estuary using observed bathymetry and validated with several observational datasets spanning the estuary. The model was able to reproduce the observed tidal dissipation characteristics including dominant semidiurnal M2

tidal amplitude decay and phase changes, as well as the nonlinear growth of the M4 and M6 harmonics. The model underestimates the spatial evolution of the M4 magnitude by about a factor of 2 in the narrows of the lower Piscataqua River, and overestimates the values in the upper reaches of the Great Bay toward the Squamscott River. This could be due to complexities in the bathymetry and sidewalls in this part of the estuary not considered in the model, or from viscous or turbulent effects assumed constant throughout the model domain, and should be the topic of further investigation. The modeled behavior reproduces a highly dissipative, partially progressive wave in the lower 12 *km* of the Piscataqua River (with 45% tidal energy loss by Dover Pt., consistent with previous observational studies; Swift and Brown, 1983), and a (nearly) standing wave in the low dissipative region between Dover Pt. and the upper reaches of the Great Bay. The spatial evolution from the mouth upstream in the estuary of the tidal harmonics, sea surface elevation skewness and asymmetry, and phase relationship between the along-channel velocity and sea surface time series, indicates a strong nonlinear tidal evolution consistent with an ebb dominant flow in the lower Piscataqua, and a flood dominant flow in the Great Bay. The good comparisons with observations suggest that the model well represents the nonlinear behavior of the tide, and accurately simulates the velocity and sea surface elevation time series throughout the estuary. Differences between model simulations with and without subtidal oscillations or river fluxes for the Great Bay are small, suggesting that interactions between the tide and other low frequency (subtidal) or baroclinic flows are weak and can be ignored when considering tidal dynamics.

Acknowledgement

Funding for this work was supported by the Office of Naval Research (ONR) Littoral Geosciences and Optics Program under grant number N00014-14-1-0557, New Hampshire Sea Grant Project R/HCE-1 under grant number NA14OAR4170083, and with funds provided by the University of New Hampshire. This research is part of the Blue Waters sustained-petascale computing project, which is supported by the National Science Foundation (awards OCI-0725070 and ACI-1238993) and the state of Illinois. Blue Waters is a joint effort of the University of Illinois at Urbana-Champaign and its National Center for Supercomputing Applications. Computations were also performed on Trillian, a Cray XE6m-200 supercomputer at the Institute for Earth, Ocean, and Space at UNH supported by NSF MRI program under grant PHY-1229408. Jon Hunt provided field assistance for the 2015 field experiments. The 2007 observations were obtained by Karl Kammerer of NOAA. Chris Sherwood of the USGS and Jamie Pringle of UNH assisted with establishing a stable model for the simulations presented.

References

Armstrong, P.B., Hanson, G.M., Gaudette, H.E., 1976. Minor elements in sediments of Great Bay Estuary, New Hampshire. Environ. Geol. 1, 207–214.
Aubrey, D., Speer, P.E., 1985. A study of non-linear tidal propagation in shallow inlet/estuarine systems. Part I: observations. Estuar. Coast. Shelf Sci. 21, 185–205.
Bendat, J.S., Piersol, A.G., 2000. Random Data: Analysis and Measurement Procedures, 3rd edition. Wiley-Interscience, New York, pp. 566.
Boon, J.D., Byrne, R.J., 1981. On basin hypsometry and the morphodynamic response of coastal inlet systems. Mar. Geol. 40 (1–2), 27–48.
Brown, W.S., Irish, J.D., 1992. The annual evolution of geostrophic flow in the Gulf of Maine: 1986–1987. J. Phys. Oceanogr. 22, 445–473.
Brown, W.S., Trask, R.P., 1980. A study of tidal energy dissipation and bottom stress in an estuary. J. Phys. Oceanogr. 10, 1742–1754.
Carter, G.S., Merrifield, M.A., 2007. Open boundary conditions for regional simulations. Ocean Model. 18, 194–209.
Chapman, D.C., 1985. Numerical treatment of cross-shelf open boundaries in a barotropic coastal ocean model. J. Phys. Oceanogr. 15, 1060–1075.
Chen, C., Liu, H., Beardsley, R.C., 2003. An unstructured grid, finite-volume, three-dimensional, primitive equations ocean model: application to coastal ocean and estuaries. J. Atmos. Ocean. Technol. 20, 159–186.
Dronkers, J., 1986. Tidal asymmetry and estuarine morphology. Neth. J. Sea Res. 20 (2/3), 117–131.
Egbert, G.D., Erofeeva, S.Y., 2002. Efficient inverse modeling of barotropic ocean tides. J. Atmos. Ocean. Technol. 19, 183–204.
Elgar, S., Guza, R.T., 1985. Observations of bispectra of shoaling surface gravity waves. J. Fluid Mech. 161, 425–448.
Erturk, S.N., Bilgili, A., Swift, M.R., Brown, W.S., Celikkol, B., 2002. Simulation of the Great Bay Estuarine System: tides with tidal flats wetting and drying. J. Geophys. Res. 107 (C5), 3038. https://doi.org/10.1029/2001JC000883.
Flather, R.A., 1976. A tidal model of the northwest European continental shelf. Mem. Soc. R. Sci. Liege 6, 141–164.
Friedrichs, C., Aubrey, D., 1988. Non-linear tidal distortion in shallow well-mixed estuaries: a synthesis. Estuar. Coast. Shelf Sci. 27, 521–545.
Garrett, C., 1972. Tidal resonance in the Bay of Fundy and Gulf of Maine. Nature. 238, 441–443.
Geyer, W.R., MacCready, P., 2014. The estuarine circulation. Annu. Rev. Fluid Mech. 46, 175–197.
Gonella, J., 1972. A rotary-component method for analyzing meteorological and oceanographic vector time series. Deep-Sea Res. 19, 833–846.
Haidvogel, D.B., Arango, H., Budgell, W.P., Cornuelle, B.D., Curchitser, E., Di Lorenzo, E., Fennel, K., Geyer, W.R., Hermann, A.J., Lanerolle, L., Levin, J., McWilliams, J.C., Miller, A.J., Moore, A.M., Powell, T.M., Shchepetkin, A.F., Sherwood, C.R., Signell, R.P., Warner, J.C., Wilkin, J., 2008. Ocean forecasting in terrain-following coordinates: formulation and skill assessment of the Regional Ocean Modeling System. J. Comput. Phys. 227, 3595–3624.
Ip, J.T.C., Lynch, D.R., Friedrichs, C.T., 1998. Simulation of estuarine flooding and dewatering, with application to Great Bay, NH. Estuar. Coast. Shelf Sci. 47, 119–141.
Kantha, L.H., Clayson, C.A., 1994. An improved mixed layer model for geophysical applications. J. Geophys. Res. 99, 25,235–25,266.
Kundu, P.K., 1990. Fluid Mechanics. 155 Academic Press, San Diego.
Lesser, G.R., Roelvink, J.A., van Kester, J.A.T.M., Stelling, G.S., 2004. Development and validation of a three-dimensional morphological model. Coastal Eng. 51, 883–915.
Lewis, M.J., Neill, S.P., Hashemi, M.R., Reza, M., 2014. Realistic wave conditions and their influenc on quantifying tidal stream energy resource. Appl. Energy 136, 495–508.
Marchesiello, P., McWilliams, J.C., Shchepetken, A., 2001. Open boundary conditions for long-term integration of regional oceanic models. Ocean Model. 3, 1–20.
McLaughlin, J.W., Bilgili, A., Lynch, D.R., 2003. Numerical modeling of tides in the Great Bay Estuarine System: dynamical balance and spring-neap residual modulation. Estuar. Coast. Shelf Sci. 57, 283–296.
Moriarty, J.M., Harris, C.K., Hadfield, M.G., 2014. A hydrodynamic and sediment transport model for the Waipoa Shelf, New Zealand: sensitivity of fluxes to spatially-varying erodibility and model nesting. J. Mar. Sci. Eng. 2, 336–369. https://doi.org/10.3390/jmse2020336.
Neill, S.P., Hashemi, M.R., Lewis, M.J., 2014. The role of tidal asymmetry in characterizing the tidal energy resource of Orkney. Renew. Energy 68, 337–350.
NHDES, 2007. New Hampshire Estuaries Project, Hydrologic parameters for New Hampshire's estuaries. Prepared by P. Trowbridge (Available at http://www.nhep.unh.edu/resources/pdf/hydrologic_parameters_for nhep_07.pdf).
Palma, E.D., Matano, R.P., 1998. On implementation of passive open boundary conditions for a general circulation model: the barotropic mode. J. Geophys. Res. 103 (C1), 1319–1341.
Palma, E.D., Matano, R.P., 2000. On implementation of passive open boundary conditions for a general circulation model: the three dimensional case. J. Geophys. Res. 105 (C4), 8605–8627.
Parker, B.B., 1984. Frictional effect on the tidal dynamics of a shallow estuary. PhD. Dissertation, The Johns Hopkins University, Baltimore, Maryland. In: 292 pages.
Parker, B.B., 1991. The relative importance of the various non-linear mechanisms in a wide range of tidal interactions (review). Tidal Hydrodynamics. John Wiley, New York. 237–268.
Pawlowicz, R., Beardsley, B., Lentz, S., 2002. Classical tidal harmonic analysis including error estimates in MATLAB using T_TIDE. Comput. Geosci. 28, 929–937.
Plant, N.G., Holland, K.T., Puleo, J.A., 2002. Analysis of the scale of errors in nearshore bathymetric data. Mar. Geol. 191, 71–86.
Shchepetkin, A.F., McWilliams, J.C., 2005. The regional oceanic modeling system (ROMS): a split-explicit, free-surface, topography-following-coordinate oceanic model. Ocean Model. 9, 347–404.
Short, F.T., 1992. The Ecology of the Great Bay Estuary, New Hampshire and Maine: An Estuarine Profile and Bibliography. NOAA – Coastal Ocean Program Publ. 222 pp.
Silver, A.L., and Brown, W.S., 1979. Great Bay estuarine field program 1975 data report Part II; temperature, salinity and density. University of New Hampshire Sea Grant Technical Report UNH-SG-167, (42 pp).
Speer, P.E., Aubrey, D., 1985. A study of non-linear tidal propagation in shallow inlet/estuarine systems. Part II: theory. Estuar. Coast. Shelf Sci. 21, 207–224.
Swenson, E., Brown, W.S., and Trask, R.P., 1977. Great Bay estuarine field program 1975 data report Part I: currents and sea levels. University of New Hampshire Sea Grant Technical Report UNH-SG-157, (109 pp).
Swift, M.R., Brown, W.S., 1983. Distribution of bottom stress and tidal energy dissipation in a well mixed estuary. Estuar. Coast. Shelf Sci. 17, 297–317.
Taylor, J.R., 1982. An Introduction to Error Analysis: The Study of Uncertainties in Physical Measurements. Mill Valley, Calif. University Science Books.
Umlauf, B.H., Burchard, H., 2003. A generic length-scale equation for geophysical turbulence models. J. Mar. Res. 61, 235–265.
Warner, J.C., Geyer, W.R., Lerczak, J.A., 2005a. Numerical modeling of an estuary: a comprehensive skill assessment. J. Geophys. Res. 110, C05001. https://doi.org/10.1029/2004JC002691.
Warner, J.C., Sherwood, C., Arango, H., Signel, R., 2005b. Performance of four turbulence closure models implemented using a generic length scale method. Ocean Model. 8, 81–113.

Warner, J.C., Sherwood, C.R., Signell, R.P., Harris, C., Arango, H.G., 2008. Development of a three dimensional, regional, coupled wave, current, and sediment-transport model. Comput. Geosci. 34, 1284–1306.
Warner, J.C., Armstrong, B., He, R., Zambone, J.B., 2010. Development of a coupled ocean–atmosphere–wave–sediment transport (COAWST) modeling system. Ocean Model. 35, 230–244.
Warner, J.C., Defne, Z., Haas, K., Arango, H., 2013. A wetting and drying scheme for ROMS. Comput. Geosci. 35, 54–61.
Wengrove, M.E., Foster, D.L., Kalnejais, L.H., Percuoco, V., Lippmann, T.C., 2015. Field and laboratory observations of bed stress and associated nutrient release in a tidal estuary. Estuar. Coast. Shelf Sci. 161, 11–24.
Westerink, J.J., Luettich, R.A., Baptists, A.M., Scheffner, N.W., Farrar, P., 1992. Tide and storm surge predictions using finite element model. J. Hydraul. Eng. 118 (10), 1373–1390.
Yang, Z., Richardson, P., Chen, Y., Kelley, J.G., Myers, E., Aikman III, F., Peng, M., Zhang, A., 2016. Model development and hindcast simulations of NOAA's Gulf of Maine Operational Forecast System. J. Mar. Sci. Eng. 4, 77.
Zhang, W.G., Wilkin, J.L., Chant, R.J., 2009. Modeling the pathways and mean dynamics of river plume dispersal in the New York Bight. J. Phys. Oceanogr. 39, 1167–1183.